Long-distance copropagation of quantum key distribution and terabit classical optical data channels

Liu-Jun Wang,[1,2] Kai-Heng Zou,[3] Wei Sun,[1,2] Yingqiu Mao,[1,2] Yi-Xiao Zhu,[3] Hua-Lei Yin,[1,2] Qing Chen,[4] Yong Zhao,[4] Fan Zhang,[3,*] Teng-Yun Chen,[1,2,†] and Jian-Wei Pan[1,2,‡]

[1]*Hefei National Laboratory for Physical Sciences at Microscale and Department of Modern Physics, University of Science and Technology of China, Hefei, Anhui 230026, China*

[2]*CAS Center for Excellence and Synergetic Innovation Center in Quantum Information and Quantum Physics, University of Science and Technology of China, Hefei, Anhui 230026, China*

[3]*State Key Laboratory of Advanced Optical Communication Systems and Networks, Peking University, Beijing 100871, China*

[4]*QuantumCTek Co., Ltd., Hefei, Anhui 230088, China*

(Received 17 October 2016; published 3 January 2017)

Quantum key distribution (QKD) generates symmetric keys between two remote parties and guarantees the keys are not accessible to any third party. Wavelength-division multiplexing between QKD and classical optical communications by sharing the existing fiber-optics infrastructure is highly desired in order to reduce the cost of QKD applications. However, comparing to the light for classical transmission, quantum signals are very weak and easily affected by impairments from classical light, such as the spontaneous Raman-scattering effect. Here, by selecting an optimal wavelength of quantum signals, we significantly reduce the influence of the Raman-scattering effect. In addition, through coherent optical communication technology, we achieve high-speed classical data transmission with relatively low launch powers, thereby further reducing the impairments from classical light. As a result, we realize the multiplexing and long-distance copropagation of QKD and terabit classical data transmission up to 80 km. The data capacity is two orders of magnitude larger than the existing results. Our demonstration verifies the feasibility of QKD and classical communication to share the resources of backbone fiber links and thus taking the utility of QKD a great step forward.

DOI: 10.1103/PhysRevA.95.012301

I. INTRODUCTION

Quantum key distribution (QKD) [1–3] supplies information-theoretic security [4] for private key exchange, based on the principles of quantum mechanics. Since its introduction in 1984 [1], tremendous progress from point-to-point experiments [5–11] to QKD network implementations [12–15] has been made. In most of the existing practical QKD systems, various single-photon sources, such as the weak coherent state source, are employed. Comparing to the light used in classical data transmission, quantum signals are very weak. The impairments from strong classical lights, such as the spontaneous Raman-scattering effect [16–19], would destroy the quantum state transmission. Thus, dark fibers are often required, which render QKD extremely expensive.

To avoid the high cost of laying extra fiber resources, the integration of QKD with conventional telecom fiber channels is of great importance. One popular solution is to multiplex QKD with classical optical channels through wavelength-division multiplexing (WDM), which was first realized by Townsend in 1997 [20] and further extended to optical access and metropolitan networks with a moderate classical bit rate of gigabits per second (Gbps) [21–29]. In addition to the BB84 QKD protocol, the continuous variable QKD has been simulated and demonstrated to be wavelength division multiplexed with classical channels [30,31] in which the classical optical power can be up to the level of 10 dBm but the transmission distance is limited to 25 km. So far, QKD has not been multiplexed into high data capacity optical backbone links. In this paper, we demonstrate that QKD can be deployed in terabit classical optical communication environments with a long-distance fiber link up to 80 km, which shows the integration feasibility of QKD and the classical telecom backbone infrastructure.

Classical backbone links have characteristics of long distances and high throughputs. For instance, a typical span distance is 80 km, and the communication capacity of one fiber link reaches up to terabits per second (Tbps) magnitude. Unfortunately, the highest experimental and field trial record of a classical data channel bandwidth used to simultaneously transmit QKD is 40 Gbps [32,33]. In fact, from the simulation results of Patel *et al.* [32], when the quantum signal's wavelength is located at the *C* band (1530–1565 nm), the maximum bandwidth of data channels achievable was predicted to be 140 Gbps. This is because that, as the bandwidth increases, the classical light launch power also increases, resulting in stronger spontaneous Raman-scattering noise and other impairments induced by the classical light, which would overwhelm the weak quantum signals even using the best spectral and temporal filtering techniques.

Here, we report a technique that can successfully reduce the spontaneous Raman-scattering noise and improve the tolerable capacity of classical data channels. On one hand, we determine the preferable wavelength for quantum signals through Raman noise measurements and QKD secure key rate simulation. Generally, the classical signal wavelength λ_c was usually chosen in the *C* band (1530–1565 nm), whereas the quantum signal wavelength λ_q was also located at the *C* band because of its low fiber loss [34–38] or at the *O* band (1260–1360 nm) because of its low Raman noise [21,22,39,40]. Hence, we need to consider the two factors together to determine the appropriate quantum signal wavelength in different classical optical communication environments.

*fzhang@pku.edu.cn
†tychen@ustc.edu.cn
‡pan@ustc.edu.cn

On the other hand, for the classical data channels, we adopt the currently popular coherent optical communication combined with M-ary quadrature amplitude modulation (QAM) formats. By using 16 and 64 QAM in our experiment, the optimal launch power is about 10 dBm at the Tbps level, and the generated Raman-scattering noise is within the acceptable range. In contrast, classical data channels in previous experiments generally used on-off keying (OOK) modulation schemes, which are intensity modulated and detected directly by photodiodes. Under this kind of modulation, a bit rate of 1 Gbps typically corresponds to a launch power of 0 dBm (1 mW). As the bit rate is basically proportional to the launch power, 1-Tbps OOK data communication would require 30-dBm classical light, which will result in the unacceptably severe Raman-scattering noise. We note that high-order QAMs require higher optical signal-to-noise ratios (OSNRs) than OOK modulations. The low launch power will lead to a worse OSNR whereas the high launch power will result in severe fiber nonlinear distortions that deteriorate the signal quality. Therefore, for a specific transmission distance, there exists an optimal launch power as a trade-off to balance the influence of noise and nonlinear interference.

In the experiment, we demonstrate that QKD can be deployed along with terabit classical optical communication with long-distance fiber links up to 80 km. This result is particularly interesting in the integration of QKD and the classical telecom backbone infrastructure.

II. RAMAN NOISE AND SECURE KEY RATES AT 1550.12 AND 1310 nm

In order to quantify the impact of Raman scattering on the QKD, we measure the forward Raman-scattering noises, which transmit in the same direction as the incident light at both 1550.12 and 1310 nm using an InGaAs avalanche photodiode- (APD-) based single-photon detector, operating at 1.25 GHz with a 180-ps full width at half maximum gate width. Figure 1 shows the count rate of Raman noise generated from a continuous-wave laser source tuned from 1530 to 1570 nm and launched with a power level of 6 dBm. We note that, in the $\lambda_q = 1550.12$-nm configuration, the QKD receiver used a 20-GHz fiber Bragg gating to filter the Raman noise, which induces an extra loss of 3.2 dB. Whereas in the $\lambda_q = 1310$-nm configuration, a bandpass filter with a center wavelength of 1310.0 nm, a passband width of 100 GHz, and an insertion loss of 0.5 dB was used. Consequently, the Raman noise at 1550.12 nm strongly depends on the incident light wavelength, which has a count rate of 440.4 kcps on average between 1550.12 ± 3 nm and two times more counts beyond 1550.12 ± 10 nm. Moreover, Fig. 1 shows the intensity of the anti-Stokes scattering slightly weaker than that of the Stokes scattering. Meanwhile, the averaged noise count rate at 1310 nm is 6.2 kcps and decreases slightly with the increasing classical signal wavelength. We can see that, although the received bandwidth of 1550.12 nm is 1/5 that of 1310 nm, the Raman noise at 1550.12 nm is approximately two orders of magnitude higher than that of 1310 nm. Nevertheless, the typical fiber attenuation at 1310 nm is 0.33 dB/km, which is larger than the loss of 0.2 dB/km at 1550.12 nm.

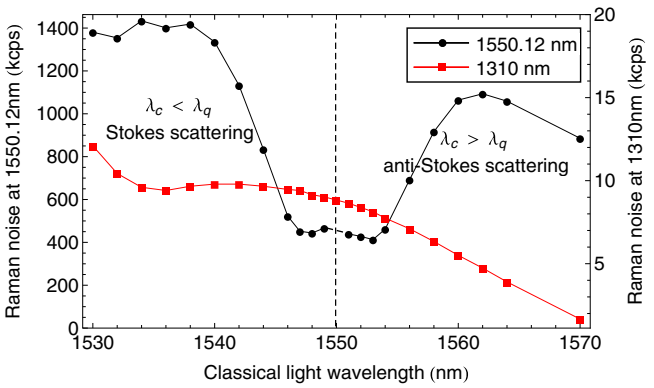

FIG. 1. Raman noise at 1550.12 nm (black circles) and 1310 nm (red squares). The forward Raman noises are measured in kilocounts per second (kcps) as a function of the classical light wavelength in a 13.6-km standard single-mode fiber at room temperature. The classical launch power is 6 dBm.

In order to compare the secure key rates of the two quantum signal wavelengths, we consider a scenario of QKD copropagating with classical channels in a 50-km fiber and simulate the key rate as a function of classical launch power as shown in Fig. 2. The Raman-scattering coefficient we used is obtained from the measured data of Raman noise in Fig. 1, and the QKD key rate simulation follows the decoy method [41] (see Appendix A for the values of the key parameters). One can see that the key rate corresponding to $\lambda_q = 1550.12$ nm is higher than that of 1310 nm when the classical launch power is less than -0.76 dBm because the Raman noise for both cases is small at low classical launch power, whereas 1550.12 nm has the advantage of low fiber loss.

As the optical launch power increases, the disturbance from Raman noise becomes evident that it deteriorates quantum signals of 1550.12 nm much more severely than that of 1310 nm, thus, resulting in its rapid key rate decline. When the launch power reaches -0.76 dBm, the key rates of both wavelengths are the same, and afterwards 1310-nm quantum

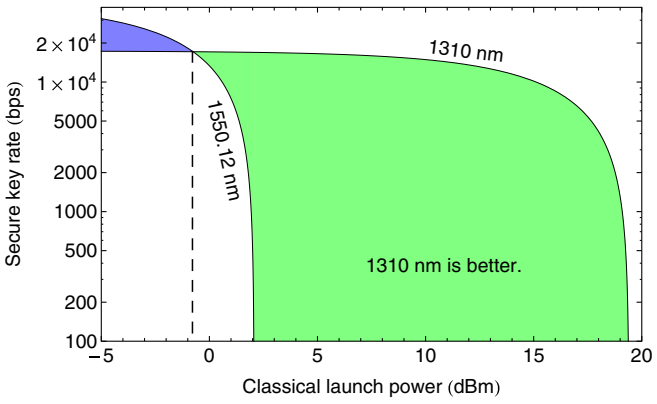

FIG. 2. Secure key rate comparison between 1550.12 and 1310 nm. The secure key rates were calculated at a 50-km fiber length as a function of classical launch power. The left blue region indicates that 1550.12 nm offers a higher key rate than 1310 nm, whereas the right green area indicates vice versa and that 1310 nm is more suitable for the quantum signal wavelength in a Tbps environment where the classical launch power is around 10 dBm.

signals display more advantages from the low level of Raman noise at 1310 nm. In addition, as we can see, when the power is greater than 2.0 dBm, 1550.12 nm could not generate any secure keys whereas 1310 nm could still perform well up to a power level of about 10 dBm, which corresponds to the Tbps level of classical communication. Similar results could be obtained for the QKD counterpropagation scenario. Consequently, we choose 1310 nm as the wavelength of quantum signals in our experiment, which not only allows one to achieve higher degrees of isolation in suppressing the linear cross talk through low-cost coarse wavelength-division multiplexers (CWDMs), but also avoids nonlinear four-wave mixing effects when multiple *C*-band classical channels are used, which may produce additional noise for a 1550.12-nm quantum channel [24,35].

III. COPROPAGATION OF QKD AND FOUR 64-QAM CLASSICAL CHANNELS

Figure 3 shows the experimental setup. Classical communication includes multiple dense-wavelength-division multiplexing network channels within the *C* band with wavelengths $\lambda_1,\lambda_2,\ldots,\lambda_{2n-1},\lambda_{2n}$. Meanwhile, our QKD system (see Appendix A) employs a polarization encoding-based BB84 protocol [1] and the decoy-state method against photon-number-splitting attacks [41–44]. The clock synchronization between the QKD transmitter and the receiver (referred to as Alice and Bob) is achieved with 100-kHz optical pulses at a wavelength of 1570 nm. The classical, the quantum, and the synchronization channels are multiplexed and demultiplexed using CWDMs to transmit over a single standard single-mode fiber. The CWDMs provide about 83-dB suppression of the in-band noise in the multiplexing and >180-dB isolation between the classical and the quantum channels in the demultiplexing, which is sufficient to reduce the linear cross talk to a negligible level. Before the detection of quantum signals, we use a custom-made 1310-nm bandpass filter with a bandwidth of 100 GHz to diminish the Raman noise down to about 1/24 of that that passes through the demultiplexing CWDMs. The single-photon detectors can also effectively reduce the Raman noise in the time domain through narrow gate widths.

In the first set of experiments, the classical optical communication system consists of four channels modulated with the 64-QAM format. The channel spacing is 50 GHz with wavelengths ranging from 1549.1 to 1550.3 nm. The bit rate of each channel is 336 Gbps, and thus the total gross data capacity is 1.344 Tbps. The co- and counterpropagating WDM layouts (see Appendix C) each induce a total loss of about 1.6 dB to classical channels. Figure 4 shows the measured classical bit error rate (BER) and Raman noise as functions of classical launch power after 50-km standard single-mode fiber transmission with QKD copropagating with classical channels in a WDM way. One can see that the classical BER is slightly higher with QKD than that of without due to the additional attenuation induced by QKD multiplexing. The BER has a minimum value at 4-dBm launch power. As

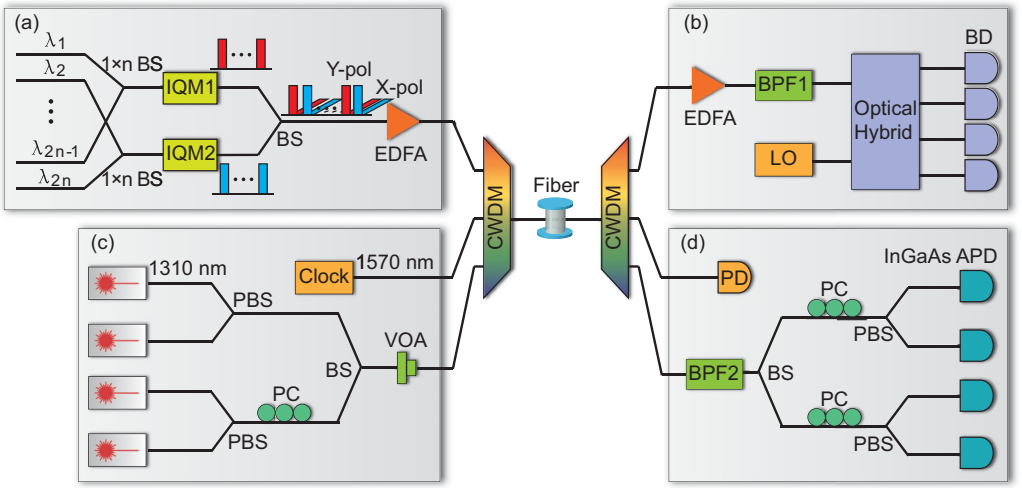

FIG. 3. Multiplexing schematic of QKD and Tbps data channels. (a) Classical transmitter. To simulate a real communication environment, we build up two sets of transmitters (see Appendix B). The odd channels are combined by a beam splitter (BS) to enter modulator 1, and the even channels are combined to enter modulator 2. Then the odd and even channels are combined in an interleaving way. The two in-phase and quadrature modulators (IQMs) are driven by electrical signals with different data sequences, ensuring the adjacent channels carrying independent data. After an emulator of polarization division multiplexing, we use an erbium-doped fiber amplifier (EDFA) to amplify and control the power of the classical light which enters the fiber link. (b) Classical receiver. At the receiver site, an EDFA amplifies the classical signals first, then a tunable bandpass filter at the *C* band (BPF1) is used to select the channel to be detected. In a polarization and phase diversity coherent receiver, the signal light and a local oscillator (LO) laser with approximately the same frequency are passed onto a polarization splitter and mixed in an optical hybrid from which we operate balanced detection (BD) using paired photodiodes to accurately extract the signal amplitude and phase information. (c) Quantum transmitter. Four nonorthogonal states are generated through two polarizing beam splitters (PBS) and a polarization controller (PC), and the incident power of the quantum states is adjusted by a variable optical attenuator (VOA). (d) Quantum receiver. We use a 100-GHz bandpass filter (BPF2) at 1310 nm to effectively suppress the Raman noise. The quantum signals are detected in two conjugate bases using InGaAs avalanche photodiode- (APD-) based single-photon detectors, and the states of polarization are controlled with automatic feedback systems.

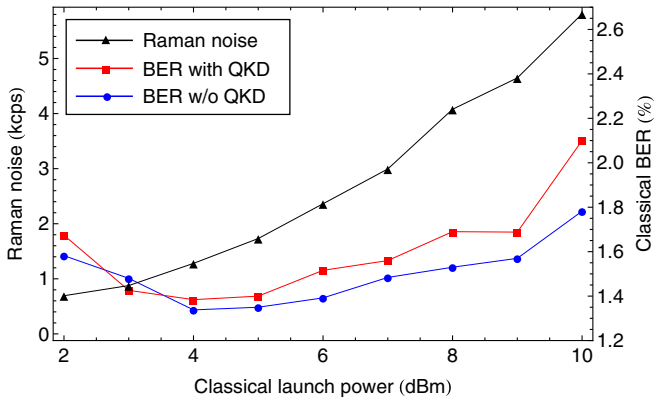

FIG. 4. The classical BER and forward Raman noise (measured at 1310 nm) as functions of classical launch power at 50 km.

the power increases, the nonlinear distortions will degrade the signal quality and thus increase the BER. In addition, as shown in Fig. 4, the amount of Raman noise generated from the classical signal at 1310 nm is proportional to the incident light power, indicating that the spontaneous Raman scattering is a linear effect.

Figure 5(a) shows the Raman noise and the classical BER measured at different fiber distances in the WDM environment. Both the forward and the backward Raman noises

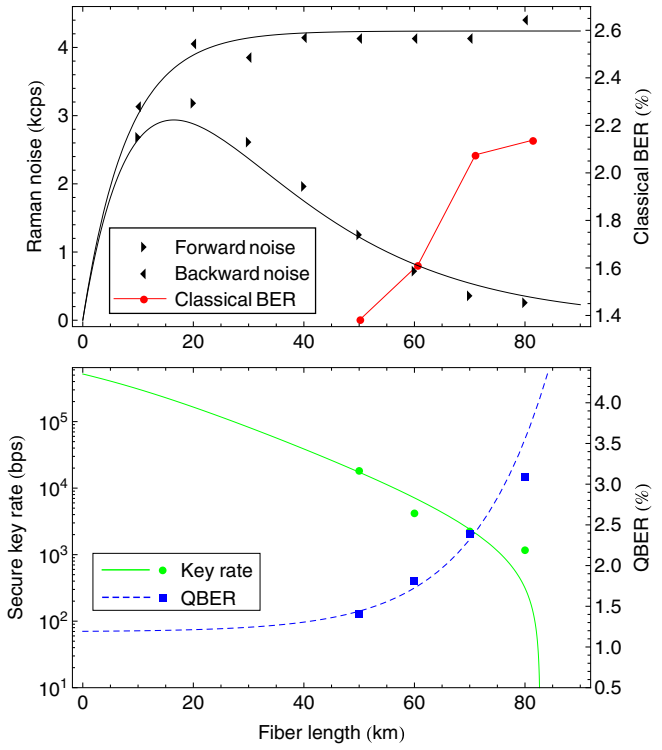

FIG. 5. Classical BER and QKD performances with WDMs. (a) Measured (triangular symbols) and simulated (solid lines) forward and backward Raman noises as a function of fiber length and the measured classical BER (red circles) with the WDM. (b) Measured and simulated QKD secure key rates (green circles and solid line) and QBER (blue squares and dashed line) with quantum signals copropagating with four classical channels.

are measured at 4-dBm launch power. As the transmission distance increases, the forward Raman noise first increases and then decreases, whereas the backward Raman noise increases gradually until saturation. Also, the backward noise count is much higher than the forward noise, which is consistent with theoretical calculations. It should be noted that, for classical communication, the forward error correction (FEC) usually is adopted, which can correct a pre-FEC BER of 0.45% or 2.4% to a level of 10^{-15} or less by adding hard- or soft-decision FEC with 7% or 20% overhead, respectively [45,46].

Since Tbps communication is generally deployed in optical trunk links, we demonstrate the copropagation of QKD and the four classical data channels at moderately longer distances. Figure 5(b) shows the QKD secure key rate and quantum bit error rate (QBER) in this scenario. The QKD secure key rate after 50-km transmission is 18.7 kbps, and the classical launch power is kept at 4 dBm from 50 to 70 km with the BER below 2.4%. The maximum distance we achieved is 80 km with a fiber loss of 27.1 dB at 1310 nm, the secure key rate is 1.2 kbps, and the QBER is 3.1%. For 80-km copropagation, we have to increase the optical power of the classical channels to 8 dBm, which is the optimal launch power in order to ensure its BER to be below 2.4% (2.14% in the experimental measurement). Considering the soft-decision FEC with 20% redundancy and frame overhead, the net bit rate of the classical communication is actually 1.07 Tbps. In the counterpropagating case, QKD suffers from much stronger backward Raman scattering. From Fig. 5(a) one can see that the backward Raman noise count at 50 km is 3.2 times more than its forward noise, resulting in a QBER of 1.98% and a key rate of 17.7 kbps. The maximum distance we achieved in the counterpropagating case is 70 km with the QBER at 2.62% and the key rate of 3.7 kbps where we have increased the classical launch power to 5 dBm with a measured BER of 2.18%(<2.4%), and the net bit rate of the classical channels is still 1.07 Tbps.

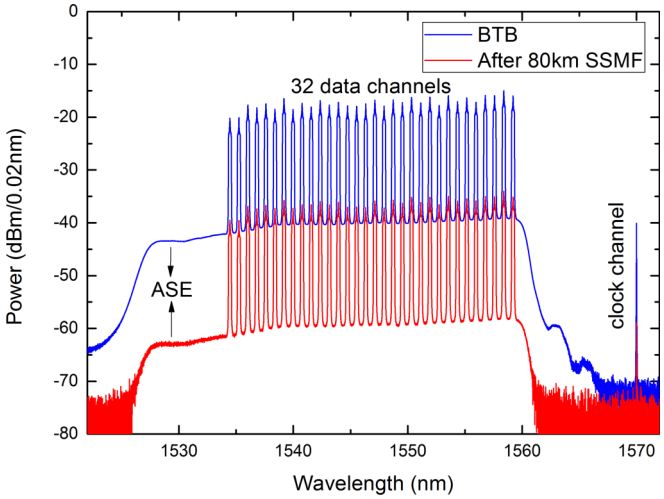

FIG. 6. The spectrum of 32 classical data channels and the QKD clock synchronous channel, which is measured back to back (BTB) as the blue (upper) line and after transmission over an 80-km standard single-mode fiber as the red (lower) line. One can see the obvious amplified spontaneous emission (ASE) generated from the EDFA which should be suppressed in advance to reduce the cross talk.

TABLE I. The results of multiplexing the QKD and 32 data channels.

Direction	Distance (km)	BER (%)	Throughput (Tbps)	QBER (%)	Key rate (kbps)
Copropagating	50	0.14	6.38	1.48	14.8
	80 (max)	0.77	5.69	4.24	1.0
Counterpropagating	50	0.14	6.38	2.08	8.7
	60 (max)	0.15	6.38	3.24	4.3

IV. COPROPAGATION OF QKD AND 32 16-QAM CLASSICAL CHANNELS

In the second set of experiments, we build up a classical optical communication system consisting of 32 channels modulated with a 16-QAM format. The channel spacing is 100 GHz with wavelengths ranging from 1535.7 to 1559.7 nm, and the optical spectrum is shown in Fig. 6. The bit rate of each channel is 224 Gbps, thus the total gross bandwidth amounts to 7.168 Tbps. The WDM layouts introduce about a 2-dB loss to the classical channels. We successfully implement the WDM of the QKD and classical communication at different fiber distances for both co- and counterpropagating cases. In Table I we list the measured results of 50 km and the maximum distance achievable.

We have measured that the optimal launch power for 50-km transmission is around 11 dBm. We obtain the classical BER to be below 0.45% when the fiber distance is less than or equal to 70 km, so we can perform the error correction by adding 7% overhead, therefore the effective throughput of the classical channels reaches 6.38 Tbps, improving two orders of magnitude compared with previous results [32,33]. We achieve maximum transmission distances of 80 and 60 km in the co- and counterpropagating cases, respectively.

V. CONCLUSION

For wavelength-division multiplexing, the main challenges of reducing Raman noise and suppressing linear cross talk are irrelevant to the implemented QKD protocol and encoding format. Therefore, although we adopt the point-to-point BB84 protocol with polarization encoding in our experiment, the WDM schemes we proposed are adaptive to QKD networks, such as the currently implementing Beijing-Shanghai quantum backbone network, and other QKD protocols, for example, differential phase-shift QKD and measurement device-independent QKD and other encoding formats, such as phase and time-bin encodings. Furthermore, our scheme may also be used by continuous variable QKD or other kinds of quantum communications when they copropagate with classical data channels over an optical fiber.

The secure key rate and transmission distance are related to the performance of single-photon detectors and the parameter estimation process. In our experiment, we use semiconductor APD-based detectors, but currently the superconducting nanowire single-photon detectors (SNSPDs) have better performances with a detection efficiency of $>70\%$ and a dark count rate of <100 counts/s. Therefore, if the detectors of our QKD system upgrade to SNSPDs, the secure key rates and transmission distances of the QKD will improve drastically. In addition, the finite key length we use to estimate parameters is 1×10^6. By increasing the statistical length we can obtain tighter parameter estimation, which would result in a higher secure key rate and a longer transmission distance.

In conclusion, we analyze the suitable wavelength for QKD transmission when multiplexed with the C-band classical optical communication and find that compared with 1550.12 nm, 1310-nm quantum signals are more adaptable in a Tbps classical data transmission environment with about 10-dBm launch power. Under this wavelength allocation, we have achieved more sufficient cross-talk isolation against classical channels using low-cost CWDMs. In addition, we employ the coherent optical communication combined with M-ary QAM formats, which significantly increase the classical channel capacity without introducing too much extra Raman-scattering noises. Consequently, we demonstrate the wavelength-division multiplexing of QKD with 16-QAM and/or 64-QAM coherent optical communication with a maximum throughput of 6.38 Tbps and a maximum transmission distance of 80 km, which is the typical span distance in classical communications. We note that, although the secure key rate at 80 km is relatively low, the key rate at 50 km is still enough for voice and text encryptions using a one-time pad, and through using SNSPDs or trusted relays we can realize farther key distributions. Due to the high capacity of coherent optical communication, it will be mainstream in the future and may be applied in metropolitan and access networks, and thus QKD can be deployed in more classical optical communication environments and provide high security applications at low costs.

ACKNOWLEDGMENTS

We thank X. Ma for reading of the paper and useful suggestions. We thank D. Wang for helpful discussions. This work has been supported by the Science and Technological Fund of Anhui Province for Outstanding Youth (Grant No. 1508085J02), the National Natural Science Foundation of China (Grant No. 61475004), and the Chinese Academy of Sciences (Grant No. XDA04030213).

APPENDIX A: QUANTUM KEY DISTRIBUTION SUBSYSTEM

Our QKD system operates at 625 MHz using polarization encoding. Alice encodes the information using weak coherent laser sources, and Bob detects the signals with InGaAs APD-based single-photon detectors. The detectors work at a gated mode with a detection efficiency of 10% and a dark count rate of 1×10^{-6} per clock cycle. To reduce the probability of afterpulsing, we set the dead time of the detectors to 200 ns. In addition, we implement the decoy-state method to avoid the multi-photon-state security issue. Alice launches the signal

states, weak decoy states, and vacuum decoy states with a probability ratio of 6:1:1, and the average photon numbers of signal and weak decoy states are 0.6 and 0.2, respectively.

In the simulation, we estimate the single-photon parameters and calculate the QBER and secure key rate following the decoy-state approach [41,47]. The QBER is given by

$$E_\mu = \frac{1}{Q_\mu}\left[\frac{1}{2}Y_0 + e_{\text{opt}}(1 - Y_0)(1 - e^{-\eta\mu})\right] \quad \text{(A1)}$$

where Q_μ and Y_0 are the probabilities of a detection event given Alice emits a signal state and a vacuum state, respectively, e_{opt} is the probability that a photon hitting the erroneous detector due to finite polarization contrast, which is about 0.5% for our system, and η is the overall transmittance, including fiber loss, 3-dB loss of Bob's optical components, and the 10% detection efficiency of single-photon detectors. In our experiment, Y_0 mainly has three components, the dark count and afterpulsing of detectors and the spontaneous Raman scattering from classical light. Meanwhile, the secure key rate per clock cycle is given by

$$R = q\{-Q_\mu f H_2(E_\mu) + Q_1[1 - H_2(e_1)] + Q_0\}, \quad \text{(A2)}$$

where q is the probability that Alice emits signal states and Alice and Bob choose the same bases, f is the inefficiency of error correction, which is about 1.25, e_1 is the estimated error rate of single-photon states, and Q_1 and Q_0 are the fractions of detection events by Bob that is due to the single-photon and vacuum ingredients of signal states, respectively. $H_2(x) = -x\log_2(x) - (1-x)\log_2(1-x)$ is the binary entropy function. The data block size we used to estimate parameters is 1 Mbit, and we consider the statistical fluctuations of five standard derivations. In the experiment, we implement the entire QKD postprocessing [48] based on hardware, including message authentication with preshared symmetric keys, error correction with a cascade algorithm [49], error verification with a cyclic redundancy check, and privacy amplification with a Toeplitz matrix [50].

APPENDIX B: CLASSICAL COMMUNICATION SUBSYSTEM

In our experiments, the classical communication subsystem conveys multichannel WDM optical signals with digital Nyquist pulse shaping [51,52]. The high-order modulation formats, such as 16 QAM and/or 64 QAM are adopted. We build two sets of transmitters and carry out transmission experiments of terabit Nyquist polarization division multiplexing (PDM) 16-QAM and/or 64-QAM signals. In our experiments, the arbitrary waveform generators (Keysight M8195A) operating at 56 Gsample/s with two-point up-sampling generate baseband signals of 28 GBd. The digital root-raised-cosine (RRC) filters with a roll-off factor of 0.1 are chosen for Nyquist pulse shaping. PDM is emulated with a polarization beam splitter and/or combiner and a tunable optical delay line. We digitize and record the received data with a real-time oscilloscope (Keysight DSA-X 96204Q) for offline digital signal processing and signal quality evaluation.

Figure 7 shows the frame structure of PDM Nyquist pulse-shaping signals. The preamble performs synchronization and channel estimation. The synchronization sequences consist of

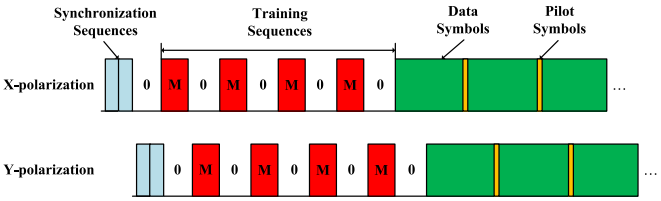

FIG. 7. Frame structure of PDM Nyquist pulse-shaping signals with time-domain training sequences.

two 63-symbol M sequences and a 130-symbol zero sequence. The training sequences (TS) for channel estimation consist of four 555-symbol M sequences, each of which is followed by a 555-symbol zero sequence. Y polarization is delayed with X polarization by 555 symbols. In each polarization, 102 400 data symbols are included after the preamble. We insert two pilots in every 512 data symbols for carrier phase correction. The total length of the preamble is 4696 symbols. The preamble is 4.59%, and the pilots are 0.39% in each frame, which are sufficient to track the time-varying channel in our experiment.

Figure 8 illustrates the DSP diagrams of the transmitter and the receiver in Nyquist pulse-shaping systems. The information data is first mapped into M-QAM format and then packed into data frames at the transmitter. After inserting pilots into the data, the preamble is inserted into the front of each frame. For 16-QAM and/or 64-QAM formats, after two samples per symbol up-sampling, both in-phase and quadrature components of the signals are digitally shaped with RRC filters. At the receiver, a finite impulse response (FIR) filter roughly compensates for the accumulated chromatic dispersion (CD). Then the carrier frequency recovery is conducted by estimating the maximum offset frequency of the fast Fourier transformation of the fourth power of the received signal [53]. A matched receiving RRC filter is adopted to satisfy the first Nyquist criterion. After synchronization, the training sequences are picked up for linear channel estimation and equalization in which time-domain FIR filterings are extracted from training sequences and convoluted with the data. The phase is corrected with pilots and then estimated with the blind phase search algorithm [54]. After phase estimation, a decision-direct recursive least-squares (DD-RLS) filter is used to improve the signal quality. To mitigate the enhanced high-frequency noise components brought by linear equalization, the signal is digitally filtered by a two-tap low-pass postfilter. Then the maximum likelihood sequence estimation (MLSE)

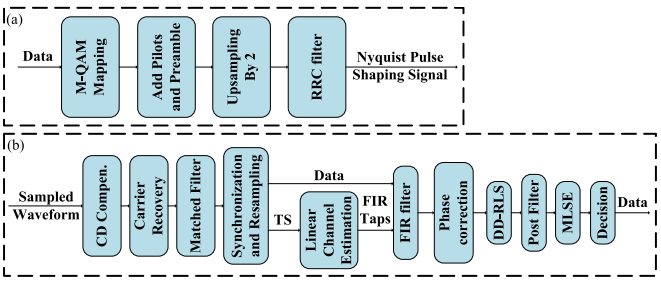

FIG. 8. Classical digital signal processing diagrams. (a) Generation of the Nyquist pulse-shaping signal. (b) Block diagrams of the receiver site digital signal processing (DSP).

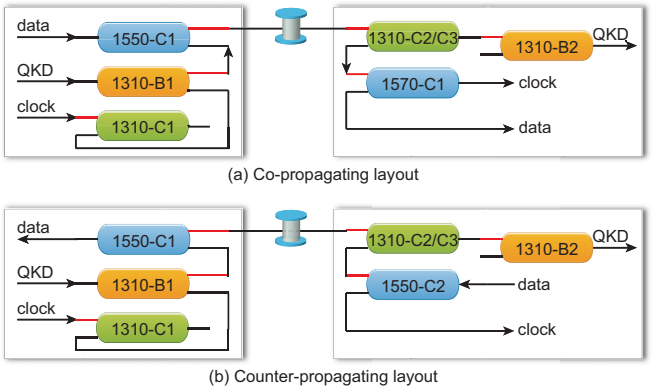

FIG. 9. The WDM layouts in the four classical channels scenario. (a) Copropagating. (b) Counterpropagating. The 1550-C1 and the 1550-C2 are 1550-nm CWDMs, 1570-C1 is a 1570-nm CWDM, 1310-C1 is a 1310-nm CWDM, 1310-C2/C3 consists of two cascaded 1310-nm CWDMs, 1310-B1 and 1310-B2 are 1310-nm bandpass filters with passband widths of 100 GHz. The common port of each filter is marked with a short red line, and the reflect port is on the same side as the common port, whereas the pass port is at the other side.

is used for the partial-response signal before the symbol decision [55].

The bit error rate is used to signal quality evaluation. For each measurement, we record a total of $\sim 10^6$ data symbols, that is, we evaluate $\sim 4 \times 10^6$ received bits for the 16-QAM signal and $\sim 6 \times 10^6$ received bits for the 64-QAM signal. To determine the BER, we perform the error counting by comparing the decoded symbols with the known bit sequence.

In our experiment, two raw BER criteria of 4.5×10^{-3} and 2.4×10^{-2} are adopted, which are the respective thresholds for error-free transmission when second-generation hard-decision FEC with 7% overhead [45] or soft-decision FEC with 20% overhead are used [46]. If the FEC works properly, the corrected output BER is less than 1×10^{-15}, which can be considered as error-free transmission.

APPENDIX C: WDM LAYOUTS

In our experiments, the WDM layouts follow the principle of guaranteeing sufficient isolation of linear cross talk and using as few filters as possible so as to reduce optical loss and cost. WDM filters generally have three ports: a common port, a pass port, and a reflect port. We find that the pass ports have much higher isolation than the reflect ports. For instance, the pass ports of 1550-nm (1310-nm) CWDMs have about 83-dB (90-dB) isolation to the light with a wavelength of 1310 nm (1550 nm), whereas the reflect ports have an isolation of only about 20 dB for the filter center wavelength. Therefore, we use one 1550-nm CWDM to suppress the in-band noise and two cascaded 1310-nm CWDMs to suppress the out-band noise, which is shown as Fig. 9. In addition, the second set of experiments has similar arrangements except that the 1550-nm CWDMs are replaced by 1550-nm filter-based wavelength-division multiplexers, which have wider pass bands to accommodate all 32 channels.

[1] C. H. Bennett and G. Brassard, Quantum cryptography: public key distribution and coin tossing, In *Proceedings of the IEEE International Conference on Computers, Systems and Signal Processing, Bangalore, India* (IEEE, New York, 1984), pp. 175–179.

[2] A. K. Ekert, Quantum Cryptography Based on Bell Theorem, Phys. Rev. Lett. **67**, 661 (1991).

[3] N. Gisin, G. Ribordy, W. Tittel, and H. Zbinden, Quantum cryptography, Rev. Mod. Phys. **74**, 145 (2002).

[4] V. Scarani *et al.*, The security of practical quantum key distribution, Rev. Mod. Phys. **81**, 1301 (2009).

[5] H. Takesue *et al.*, Quantum key distribution over a 40-dB channel loss using superconducting single-photon detectors, Nat. Photonics **1**, 343 (2007).

[6] D. Stucki *et al.*, High rate, long-distance quantum key distribution over 250 km of ultra low loss fibres, New J. Phys. **11**, 075003 (2009).

[7] A. R. Dixon, Z. L. Yuan, J. F. Dynes, A. W. Sharpe, and A. J. Shields, Continuous operation of high bit rate quantum key distribution, Appl. Phys. Lett. **96**, 161102 (2010).

[8] Y. Liu *et al.*, Decoy-state quantum key distribution with polarized photons over 200 km, Opt. Express **18**, 8587 (2010).

[9] S. Wang *et al.*, 2 GHz clock quantum key distribution over 260 km of standard telecom fiber, Opt. Lett. **37**, 1008 (2012).

[10] A. Tanaka *et al.*, High-speed quantum key distribution system for 1-Mbps real-time key generation, IEEE J. Quantum Electron. **48**, 542 (2012).

[11] B. Korzh *et al.*, Provably secure and practical quantum key distribution over 307 km of optical fibre, Nat. Photonics **9**, 163 (2015).

[12] M. Peev *et al.*, The SECOQC quantum key distribution network in Vienna, New J. Phys. **11**, 075001 (2009).

[13] T. Y. Chen *et al.*, Metropolitan all-pass and inter-city quantum communication network, Opt. Express **18**, 27217 (2010).

[14] M. Sasaki *et al.*, Field test of quantum key distribution in the Tokyo QKD Network, Opt. Express **19**, 10387 (2011).

[15] B. Fröhlich *et al.*, A quantum access network, Nature (London) **501**, 69 (2013).

[16] J. Auyeung, and A. Yariv, Spontaneous and stimulated Raman scattering in long low loss fibers, IEEE J. Quantum Electron. **14**, 347 (1978).

[17] D. Subacius, A. Zavriyev, and A. Trifonov, Backscattering limitation for fiber-optic quantum key distribution systems, Appl. Phys. Lett. **86**, 011103 (2005).

[18] G. B. Xavier, G. V. de Faria, G. P. Temporão, and J. P. von der Weid, Scattering effects on QKD employing simultaneous classical and quantum channels in telecom optical fibers in the C-band, *Quantum Communication, Measurement and Computing (QCMC): Ninth International Conference on QCMC*, 327–330 (AIP, New York, 2009).

[19] T. F. da Silva, G. B. Xavier, G. P. Temporão, and J. P. von der Weid, Impact of Raman scattered noise from multiple telecom

channels on fiber-optic quantum key distribution systems, J. Lightwave Technol. **32**, 2332 (2014).
[20] P. D. Townsend, Simultaneous quantum cryptographic key distribution and conventional data transmission over installed fibre using wavelength-division multiplexing, Electron. Lett. **33**, 188 (1997).
[21] T. E. Chapuran *et al.*, Optical networking for quantum key distribution and quantum communications, New J. Phys. **11**, 105001 (2009).
[22] I. Choi, R. J. Young, and P. D. Townsend, Quantum information to the home, New J. Phys. **13**, 063039 (2011).
[23] I. Choi, R. J. Young, and P. D. Townsend, Quantum key distribution on a 10Gb/s WDM-PON, Opt. Express **18**, 9600 (2010).
[24] N. A. Peters *et al.*, Dense wavelength multiplexing of 1550 nm QKD with strong classical channels in reconfigurable networking environments, New J. Phys. **11**, 045012 (2009).
[25] D. Lancho, J. Martinez, D. Elkouss, M. Soto, and V. Martin, QKD in standard optical telecommunications networks, *Quantum Communication and Quantum Networking* (Springer, Berlin, Heidelberg, 2010), pp. 142–149.
[26] J. Mora *et al.*, Simultaneous transmission of 20x2 WDM/SCM-QKD and 4 bidirectional classical channels over a PON, Opt. Express **20**, 16358 (2012).
[27] S. Aleksic *et al.*, Quantum key distribution over optical access networks, *Proceedings of the 18th European Conference on Network and Optical Communications, Graz, Austria* (IEEE, Piscataway, NJ, 2013), pp. 11–18.
[28] A. Ciurana *et al.*, Quantum metropolitan optical network based on wavelength division multiplexing, Opt. Express **22**, 1576 (2014).
[29] S. Aleksic *et al.*, Perspectives and limitations of QKD integration in metropolitan area networks, Opt. Express **23**, 10359 (2015).
[30] B. Qi, W. Zhu, L. Qian, and H.-K. Lo, Feasibility of quantum key distribution through a dense wavelength division multiplexing network, New J. Phys. **12**, 103042 (2010).
[31] R. Kumar, H. Qin, and R. Allaume, Coexistence of continuous variable QKD with intense DWDM classical channels, New J. Phys. **17**, 043027 (2015).
[32] K. A. Patel *et al.*, Quantum key distribution for 10 Gb/s dense wavelength division multiplexing networks, Appl. Phys. Lett. **104**, 051123 (2014).
[33] I. Choi *et al.*, Field trial of a quantum secured 10 Gb/s DWDM transmission system over a single installed fiber, Opt. Express **22**, 23121 (2014).
[34] T. J. Xia *et al.*, In-band quantum key distribution (QKD) on fiber populated by high-speed classical data channels, *Optical Fiber Communication Conference, Anaheim, CA 2006* (Optical Society of America, Washington, DC, 2006), paper no. OTuJ7.
[35] P. Eraerds, N. Walenta, M. Legré, N. Gisin, and H. Zbinden, Quantum key distribution and 1 Gbps data encryption over a single fibre, New J. Phys. **12**, 063027 (2010).
[36] K. A. Patel, J. F. Dynes, I. Choi, A. W. Sharpe, A. R. Dixon, Z. L. Yuan, R. V. Penty, and A. J. Shields, Coexistence of High-Bit-Rate Quantum Key Distribution and Data on Optical Fiber, Phys. Rev. X **2**, 041010 (2012).
[37] N. Walenta *et al.*, A fast and versatile quantum key distribution system with hardware key distillation and wavelength multiplexing, New J. Phys. **16**, 013047 (2014).
[38] L.-J. Wang *et al.*, Experimental multiplexing of quantum key distribution with classical optical communication, Appl. Phys. Lett. **106**, 081108 (2015).
[39] R. J. Runser *et al.*, Demonstration of 1.3 μm quantum key distribution (QKD) compatibility with 1.5 μm metropolitan wavelength division multiplexed (WDM) systems, *Optical Fiber Communication Conference* (Optical Society of America, Washington, DC, 2005), paper no. OWI2.
[40] N. I. Nweke *et al.*, Experimental characterization of the separation between wavelength-multiplexed quantum and classical communication channels, Appl. Phys. Lett. **87**, 174103 (2005).
[41] X. F. Ma, B. Qi, Y. Zhao, and H. K. Lo, Practical decoy state for quantum key distribution, Phys. Rev. A **72**, 012326 (2005).
[42] W. Y. Hwang, Quantum Key Distribution With High Loss: Toward Global Secure Communication, Phys. Rev. Lett. **91**, 057901 (2003).
[43] H. K. Lo, X. F. Ma, and K. Chen, Decoy State Quantum Key Distribution, Phys. Rev. Lett. **94**, 230504 (2005).
[44] X. B. Wang, Beating the Photon-Number-Splitting Attack in Practical Quantum Cryptography, Phys. Rev. Lett. **94**, 230503 (2005).
[45] F. Chang, K. Onohara, and T. Mizuochi, Forward error correction for 100 G transport networks, IEEE Commun. Mag. **48**, S48 (2010).
[46] D. Chang *et al.*, FPGA verification of a single QC-LDPC code for 100 Gb/s optical systems without error floor down to BER of 10^{-15}, *Optical Fiber Communication Conference* (Optical Society of America, Washington, DC, 2011), paper no. OTuN2.
[47] H.-K. Lo, Getting something out of nothing, Quantum Inf. Comput. **5**, 413 (2005).
[48] C.-H. F. Fung, X. Ma, and H. Chau, Practical issues in quantum-key-distribution postprocessing, Phys. Rev. A **81**, 012318 (2010).
[49] G. Brassard and L. Salvail, Secret-key reconciliation by public discussion, in *Advances in Cryptology—Proceedings of the EUROCRYPT '93: Workshop on the Theory and Application of Cryptographic Techniques Lofthus, Norway, 1993*, edited by T. Helleseth (Springer, Berlin/Heidelberg, 1994), pp. 410–423.
[50] C. H. Bennett, G. Brassard, C. Crepeau, and U. M. Maurer, Generalized privacy amplification, IEEE Trans. Inf. Theory **41**, 1915 (1995).
[51] R. Schmogrow *et al.*, Real-time Nyquist pulse generation beyond 100 Gbit/s and its relation to OFDM, Opt. Express **20**, 317 (2012).
[52] X. Zhou *et al.*, PDM-Nyquist-32QAM for 450-Gb/s per-channel WDM transmission on the 50 GHz ITU-T grid, J. Lightwave Technol. **30**, 553 (2012).
[53] S. J. Savory, G. Gavioli, R. I. Killey, and P. Bayvel, Electronic compensation of chromatic dispersion using a digital coherent receiver, Opt. Express **15**, 2120 (2007).
[54] T. Pfau, S. Hoffmann, and R. Noé, Hardware-Efficient coherent digital receiver concept with feedforward carrier recovery for M-QAM constellations, J. Lightwave Technol. **27**, 989 (2009).
[55] J. Li, E. Tipsuwannakul, T. Eriksson, M. Karlsson, and P. A. Andrekson, Approaching Nyquist limit in WDM systems by low-complexity receiver-side duobinary shaping, J. Lightwave Technol. **30**, 1664 (2012).